

# Relating the inhomogeneous power spectrum to the CMB hemispherical anisotropy

Pranati K. Rath<sup>1,a</sup>, Pavan K. Aluri<sup>2,b</sup>, and Pankaj Jain<sup>1,c</sup>

<sup>1</sup> *Dept. of Physics, Indian Institute of Technology Kanpur, Kanpur - 208016, India and*

<sup>2</sup> *IUCAA, Post Bag 4, Ganeshkhind, Pune University Campus, Pune - 411007, India*

We relate the observed hemispherical anisotropy in the cosmic microwave radiation data to an inhomogeneous power spectrum model. The hemispherical anisotropy can be parameterized in terms of the dipole modulation model. This model leads to correlations between spherical harmonic coefficients corresponding to multipoles,  $l$  and  $l + 1$ . We extract the  $l$  dependence of the dipole modulation amplitude,  $A$ , by making a fit to the WMAP and PLANCK CMBR data. We propose an inhomogeneous power spectrum model and show that it also leads to correlations between multipoles,  $l$  and  $l + 1$ . The model parameters are determined by making a fit to the data. The spectral index of the inhomogeneous power spectrum is found to be consistent with zero.

---

<sup>a</sup> Email:pranati@iitk.ac.in

<sup>b</sup> Email:aluri@iucaa.ernet.in

<sup>c</sup> Email:pkjain@iitk.ac.in

## I. INTRODUCTION

The cosmic microwave background radiation (CMBR) shows a hemispherical power asymmetry with excess power in the southern ecliptic hemisphere compared to northern ecliptic hemisphere [1–9]. The signal is seen both in WMAP and PLANCK data and indicates a potential violation of the cosmological principle. The hemispherical anisotropy can be parametrized phenomenologically by the dipole modulation model [10–13] of the CMBR temperature field, which is given by,

$$\Delta T(\hat{n}) = f(\hat{n}) \left( 1 + A \hat{\lambda} \cdot \hat{n} \right), \quad (1)$$

where  $f(\hat{n})$  is an intrinsically isotropic and Gaussian random field and,  $A$  is the amplitude of modulation along the direction  $\hat{\lambda}$ . Taking the preferred direction along the z-axis, we have  $\hat{\lambda} \cdot \hat{n} = \cos \theta$ . Using the WMAP five year data, the dipole amplitude for  $l \leq 64$  was found to be  $A = 0.072 \pm 0.022$  and the dipole direction,  $(l, b) = (224^\circ, -22^\circ) \pm 24^\circ$ , in the galactic coordinate system [5]. The PLANCK results [7] confirmed this anisotropy with a significance of  $3\sigma$  confidence level. A dipole amplitude,  $A = 0.073 \pm 0.010$ , in the direction of  $(l, b) = (217^\circ, -20^\circ) \pm 15^\circ$  was found in PLANCK's SMICA map, which is also seen (nearly with same amplitude and direction) in other PLANCK provided clean CMB maps viz., NILC, SEVEM and COMMANDER-RULER maps. Hence the results obtained by WMAP and PLANCK observations are consistent with one another. There were indications that the hemispherical anisotropy might extend to multipoles higher than 64 [4, 5], however, the effect is found to be absent beyond  $l \sim 500$  [14, 15]. The large scale structure surveys also do not show any evidence for this anisotropy [16, 17]. This suggests that any model which attempts to explain these observations should display a scale dependent power [18] which should lead to a negligible effect at high- $l$ .

There also exist other observations which indicate a potential violation of the cosmological principle [19–25]. Many theoretical models, which aim to explain the observed large scale anisotropy, have been proposed [26–50]. It has also been suggested that this anisotropy may not really be in disagreement with the inflationary Big Bang cosmology, which may have a phase of anisotropic and inhomogeneous expansion at very early time. The anisotropic modes, generated during this early phase may later re-enter the horizon [51, 52] and lead to the observed signals of anisotropy.

In a recent paper [53], we showed that the dipole modulation model, given in Eq. 1, leads to several implications for CMBR. The CMBR temperature field may be decomposed as,

$$\Delta T(\hat{n}) = \sum_{lm} a_{lm} Y_{lm}(\hat{n}). \quad (2)$$

If we assume statistical isotropy, the spherical harmonic coefficients must satisfy,

$$\langle a_{lm} a_{l'm'}^* \rangle_{iso} = C_l \delta_{ll'} \delta_{mm'}, \quad (3)$$

where,  $C_l$  is the angular power spectrum. However in the presence of dipole modulation, statistical isotropy is violated and one finds [53],

$$\langle a_{lm} a_{l'm'}^* \rangle = \langle a_{lm} a_{l'm'}^* \rangle_{iso} + \langle a_{lm} a_{l'm'}^* \rangle_{dm}, \quad (4)$$

where,  $\langle a_{lm} a_{l'm'}^* \rangle_{iso}$  is the correlation given in Eq. 3 and the anisotropic *dipole modulation* term can be expressed as,

$$\langle a_{lm} a_{l'm'}^* \rangle_{dm} = A (C_{l'} + C_l) \xi_{lm;l'm'}^0. \quad (5)$$

Here,  $\xi_{lm;l'm'}^0$  is given by,

$$\begin{aligned} \xi_{lm;l'm'}^0 &\equiv \int d\Omega Y_l^{m*}(\hat{n}) Y_{l'}^{m'}(\hat{n}) \cos \theta \\ &= \delta_{m',m} \left[ \sqrt{\frac{(l-m+1)(l+m+1)}{(2l+1)(2l+3)}} \delta_{l',l+1} \right. \\ &\quad \left. + \sqrt{\frac{(l-m)(l+m)}{(2l+1)(2l-1)}} \delta_{l',l-1} \right]. \end{aligned} \quad (6)$$

Hence the modes corresponding to the multipoles,  $l$  and  $l+1$  are correlated. We thus define a correlation function [53],

$$C_{l,l+1} = \frac{l(l+1)}{2l+1} \sum_{m=-l}^l a_{lm} a_{l+1,m}^*. \quad (7)$$

Here the factor  $(2l+1)$  arises in the denominator in order to obtain an average value of the correlation for a particular  $l$ . Furthermore we multiply by  $l(l+1)$  since for low  $l$  the power  $l(l+1)C_l$  is approximately independent of  $l$ . Using Eq. 5 we deduce that with this factor the correlation  $C_{l,l+1}$  would be roughly equal for different  $l$  values. Analogously, the signal of hemispherical asymmetry is also observed in the variable  $l(l+1)C_l$  [1, 2]. We define the statistic,  $S_H(L)$ , by summing over a range of multipoles,

$$S_H(L) = \sum_{l=l_{min}}^L C_{l,l+1}. \quad (8)$$

We point out that if the factor  $l(l+1)$  was not inserted in Eq. 7 then the statistic will be dominated by a few low  $l$  multipoles. The final value of the data statistic is obtained by maximizing it over the direction parameters. We make a search over the direction parameters in order to maximize the value of the statistic,  $S_H(L)$ . The resulting statistic is labelled as  $S_H^{data}$ . The corresponding direction gives us the preferred direction,  $\hat{\lambda}$ , defined in Eq. 1, which corresponds to the choice of z-axis.

In this paper, our objective is twofolds:

1. We first update our results in Ref. [53] for the estimate of the effective value of the dipole modulation parameter,  $A$ , as a function of  $l$ . The multipole dependence of  $A$  in Ref. [53] was extracted using the dipole power of the temperature squared field. In the current paper we instead use the statistic,  $S_H(L)$ , which is a much more sensitive probe of  $A$  in comparison to temperature square power. In particular, this statistic leads to a higher significance of the signal of dipole modulation. Furthermore in Ref. [53], we used COM-MASK-gal-07 for the PLANCK data. In the present paper we use the KQ85 mask for WMAP's nine year ILC map and the more reliable, CMB-union mask for SMICA, also known as the U73 mask.
2. We also propose a general inhomogeneous primordial power spectrum model. This is presented in the next section, where we argue that the inhomogeneous contribution to the power spectrum in any model must reduce to ours, as long as it is small. The assumption of small inhomogeneity is reasonable and also supported by our fit to data. An inhomogeneous power model is expected to induce an anisotropy in the CMBR as well as in other cosmological observations. We show that our model leads to correlations among the spherical harmonic coefficients similar to those implied by the dipole modulation model. This allows us to relate the inhomogeneous primordial power spectrum with the dipole modulated temperature field and hence the hemispherical anisotropy. We determine the primordial power spectrum which leads to the hemispherical power asymmetry observed in the CMB temperature data.

The observed anisotropy is parametrized by the two point correlations given by Eq. 5, or equivalently the statistic,  $S_H(L)$ . We first determine the data statistic,  $S_H^{data}$ , as defined above after Eq. 8. We next determine the amplitude,  $A$ , of the dipole modulation model given by Eq. 1, by making a fit to data. We perform this analysis for the entire multipole range  $l = 2 - 64$  and also, independently, over the three multipole ranges,  $l = 2 - 22, 23 - 43, 44 - 64$ . This allows us to determine the variation of  $S_H^{data}$  and hence the dipole modulation amplitude,  $A$ , with the multipole bin. We determine the value of  $A$  by simulations, as explained in section III. The upper limit on  $l$  ( $l \leq 64$ ) is imposed since the amplitude of the dipole modulation using hemispherical analysis, has been studied most thoroughly only in this range [5, 7]. As discussed in the next section, the theoretical analysis is also simplest for low- $l$  modes. In this case we can make a simple approximation for the transfer function. At higher  $l$  the transfer function is not as simple and the computation of the correlation,  $\langle a_{lm} a_{l'm'}^* \rangle$ , in the presence of inhomogeneous and/or anisotropic is significantly more complicated. Furthermore, as we shall see, the contribution due to detector noise is negligible in the range,  $l \leq 64$ . This leads to considerable simplification in our analysis. Simulations at higher  $l$  also require much higher computation time. Finally, as we have discussed above, the signal of dipole modulation is expected to die down for values of  $l$  beyond a few hundred [14–17]. We hope to extend our analysis to higher values of  $l$  in a future publication.

We finally determine the inhomogeneous power spectrum by making a fit to the data statistic,  $S_H^{data}$ . This calculation is also performed over the entire multipole range,  $l = 2 - 64$ , and then repeated over the three multipole bins mentioned above. Hence we determine the magnitude as well as the wave number,  $k$ , dependence of the power spectrum. The possibility of inhomogeneous power has been considered earlier, for example, in Ref. [3, 16, 38, 54]. However our analysis and results differ from these earlier papers.

## II. THEORY

The temperature fluctuations,  $\Delta T(\hat{n})$ , arise due to primordial density perturbations,  $\delta(\vec{k})$ . They can be expressed as,

$$\frac{\Delta T}{T_0}(\hat{n}) = \int d^3k \sum_l (-i)^l (2l+1) \delta(k) \Theta_l(k) P_l(\hat{k} \cdot \hat{n}), \quad (9)$$

where  $P_l(\hat{k} \cdot \hat{n})$  are the Legendre polynomials and  $\Theta_l(k)$  the transfer function. On large distance scales, i.e. low- $l$ , the main contribution to the temperature fluctuation arises from the Sachs-Wolfe effect. Hence we approximate the transfer function as  $\Theta_l(k) = \frac{3}{10} j_l(k\eta_0)$  [55], where  $j_l$  is the spherical Bessel function and  $\eta_0$  the current conformal time. A more detailed analysis is postponed to future work. Let  $\tilde{\delta}(\vec{x})$  represent the density fluctuations in real space. The two point correlation function,  $F(\vec{\Delta}, \vec{X})$ , in real space can be expressed as,

$$F(\vec{\Delta}, \vec{X}) = \langle \tilde{\delta}(\vec{x}) \tilde{\delta}(\vec{x}') \rangle, \quad (10)$$

where we have defined the variables,  $\vec{\Delta} = \vec{x} - \vec{x}'$  and  $\vec{X} = (\vec{x} + \vec{x}')/2$ . The corresponding correlation function of the Fourier transform,  $\delta(\vec{k})$ , may be expressed as,

$$\langle \delta(\vec{k}) \delta^*(\vec{k}') \rangle = \int \frac{d^3X}{(2\pi)^3} \frac{d^3\Delta}{(2\pi)^3} e^{i(\vec{k}+\vec{k}') \cdot \vec{\Delta}/2} e^{i(\vec{k}-\vec{k}') \cdot \vec{X}} F(\vec{\Delta}, \vec{X}). \quad (11)$$

If we assume that  $F(\vec{\Delta}, \vec{X})$  depends only on the magnitude  $\Delta \equiv |\vec{\Delta}|$ , we obtain the standard form of the power spectrum,  $\langle \delta(\vec{k}) \delta^*(\vec{k}') \rangle = P(k) \delta^3(\vec{k} - \vec{k}')$ , where,  $k \equiv |\vec{k}|$ . An inhomogeneous model of power spectrum must necessarily depend on  $\vec{X}$  in real space. Hence for such a model  $F(\vec{\Delta}, \vec{X})$  cannot be independent of  $\vec{X}$ . Our procedure of obtaining an inhomogeneous power spectrum in Fourier space by using guidance from the real space power spectrum is similar to that followed in Ref. [38]. However the precise model we use is different from theirs.

We next assume a simple inhomogeneous model of  $F(\vec{\Delta}, \vec{X})$ . It is simplest to consider an inhomogeneous model in order to obtain the observed signal of hemispherical anisotropy or dipole modulation. An anisotropic model leads to correlations between multipoles,  $l$  and  $l+2$  [56], in contrast to the prediction based on the dipole modulation model. Hence it does not lead to the observed anisotropy. An inhomogeneous model of power spectrum in Fourier space must show dependence on the position vector,  $\vec{X}$ , in real space. We assume that our inhomogeneous model has a very mild dependence on  $\vec{X}$ . Hence we can make a Taylor expansion about any chosen origin and keep only the leading order term. We can, therefore, express  $F(\vec{\Delta}, \vec{X})$  as,

$$F(\vec{\Delta}, \vec{X}) = F(\vec{\Delta}, 0) + X_i \left. \frac{\partial}{\partial X_i} F(\vec{\Delta}, \vec{X}) \right|_{\vec{X}=0} \quad (12)$$

The Taylor expansion is justified if the second term is significantly smaller than the first. As we shall see, this expectation is validated in our numerical results. The first term on the right hand side corresponds to the standard homogeneous and isotropic power spectrum. Hence it should be a function only of the magnitude,  $\Delta$ . We parametrize it as,

$$F(\vec{\Delta}, 0) \equiv f_1(\Delta) \quad (13)$$

The second term on the right hand side in Eq. 12 represents the contribution to power spectrum due to inhomogeneity. We parametrize the derivative term as,

$$\left. \frac{\partial}{\partial X_i} F(\vec{\Delta}, \vec{X}) \right|_{\vec{X}=0} \equiv \hat{\lambda}_i \left( \frac{1}{\eta_0} f_2(\Delta) \right) \quad (14)$$

where  $f_2(\Delta)$  depends only on the magnitude,  $\Delta$ ,  $\hat{\lambda}$  is a unit vector and we have introduced a factor  $\eta_0$  in order to make the function  $f_2(\Delta)$  have same dimensions as  $f_1(\Delta)$ . We point out that since  $\vec{X}$  has dimensions of length,  $\vec{X}/\eta_0$  is dimensionless. Here  $f_2(\Delta)$  depends only on the magnitude  $\Delta$ , since otherwise the model will give an additional anisotropic contribution to the power spectrum beside the inhomogeneity. We finally obtain,

$$F(\vec{\Delta}, \vec{X}) = f_1(\Delta) + \hat{\lambda} \cdot \vec{X} \left( \frac{1}{\eta_0} f_2(\Delta) \right), \quad (15)$$

It is clear that the inhomogeneous contribution to the power spectrum in any model can be expressed in this form by making a Taylor expansion, provided the inhomogeneity is small. This of course assumes that the model does not contain any other source of violation of the cosmological principle besides the presence of inhomogeneity. The smallness of the second term implies that  $f_2(\Delta)$  is sufficiently small so that it gives a contribution smaller than the first term.

In applications to CMBR, we need to compute the correlation in Fourier space, given in Eq. 11. We express the correlation as,

$$\langle \delta(\vec{k}) \delta^*(\vec{k}') \rangle = \tilde{F}_0(\vec{k}, \vec{k}') + \Delta \tilde{F}(\vec{k}, \vec{k}'), \quad (16)$$

where  $\tilde{F}_0(\vec{k}, \vec{k}')$  and  $\Delta \tilde{F}(\vec{k}, \vec{k}')$  are, respectively, the contributions due to the homogeneous and inhomogeneous terms in Eq. 15. The first term is given by,

$$\tilde{F}_0(\vec{k}, \vec{k}') = P(k) \delta^3(\vec{k} - \vec{k}'), \quad (17)$$

where  $P(k)$  is the Fourier transform of  $f_1(\Delta)$ . We choose  $P(k)$ , or equivalently  $f_1(\Delta)$ , to be the standard power spectrum in an homogeneous and isotropic model.

We next need the Fourier transform of the inhomogeneous term. This calculation is facilitated by noting that,

$$\int \frac{d^3 X}{(2\pi)^3} X_i e^{i\vec{k}_- \cdot \vec{X}} = \int \frac{d^3 X}{(2\pi)^3} \frac{\partial}{\partial k_{-i}} e^{i\vec{k}_- \cdot \vec{X}} = -i \frac{\partial}{\partial k_{-i}} \delta^3(\vec{k}_-), \quad (18)$$

where  $\vec{k}_- = \vec{k} - \vec{k}'$ . Hence we obtain,

$$\Delta \tilde{F}(\vec{k}, \vec{k}') = -i \hat{\lambda}_i \left[ \frac{\partial}{\partial k_{-i}} \delta^3(\vec{k}_-) \right] g(\vec{k}_+), \quad (19)$$

where,

$$g(k_+) = \frac{1}{\eta_0} \int \frac{d^3 \Delta}{(2\pi)^3} e^{i\vec{k}_+ \cdot \vec{\Delta}} f_2(\Delta) \quad (20)$$

and  $\vec{k}_+ = (\vec{k} + \vec{k}')/2$ . The inhomogeneous nature of  $\Delta \tilde{F}(\vec{k}, \vec{k}')$  can be seen by the fact that it is proportional to the derivative of the delta function. We see directly from Eq. 11 that a homogeneous model of power spectrum must be proportional to  $\delta^3(\vec{k} - \vec{k}')$  since it must be independent of  $\vec{X}$  in real space [38].

The spherical harmonic coefficients,  $a_{lm}$ , of the temperature field can be expressed as,

$$a_{lm} = \int d\Omega Y_{lm}^*(\hat{n}) \Delta T(\hat{n}). \quad (21)$$

Using Eq. 9 and the identity,

$$P_l(\hat{n} \cdot \hat{n}') = \frac{4\pi}{2l+1} \sum_m Y_{lm}(\hat{n}) Y_{lm}^*(\hat{n}'), \quad (22)$$

we obtain,

$$a_{lm} = (-i)^l (4\pi T_0) \int d^3 k \delta(k) \Theta_l(k) Y_{lm}^*(\hat{k}). \quad (23)$$

We take the preferred direction,  $\hat{\lambda}$  along z-axis, i.e.  $\hat{\lambda} = \hat{z}$ . The two point correlation function of the spherical harmonic coefficients,  $a_{lm}$ , can be expressed as,

$$\langle a_{lm} a_{l'm'}^* \rangle = (4\pi T_0)^2 \int d^3 k d^3 k' (-i)^{l-l'} \Theta_l(k) \Theta_{l'}(k') Y_{lm}^*(\hat{k}) Y_{l'm'}(\hat{k}') \langle \delta(\vec{k}) \delta^*(\vec{k}') \rangle. \quad (24)$$

We parameterize this correlation as,

$$\langle a_{lm} a_{l'm'}^* \rangle = C_l \delta_{ll'} \delta_{mm'} + A(l, l'), \quad (25)$$

where  $C_l$  is the standard power spectrum arising due to the homogeneous term, given in Eq. 17, and  $A(l, l')$  represents the anisotropic part arising due to the inhomogeneous term. Setting,  $\Theta_l(k) = 3j_l(k\eta_0)/10$ , the isotropic part is given by,

$$C_l = (4\pi)^2 \frac{9T_0^2}{100} \int_0^\infty k^2 dk j_l^2(k\eta_0) P(k). \quad (26)$$

For the anisotropic part, using Eq. 16 and Eq. 19, we obtain,

$$A(l, l') = (4\pi T_0)^2 \int d^3k d^3k' (-i)^{l-l'+1} \Theta_l(k) \Theta_{l'}(k') Y_{lm}^*(\hat{k}) Y_{l'm'}(\hat{k}') g(k_+) \left( \frac{\partial}{\partial k_{-z}} \delta^3(\vec{k}_-) \right). \quad (27)$$

This can be computed by integration by parts. The details are given in Appendix A. The surface term vanishes and we obtain,

$$A(l, l') = -(4\pi T_0)^2 \int d^3k d^3k' (-i)^{l-l'+1} \delta^3(\vec{k}_-) g(k_+) \frac{\partial}{\partial k_{-z}} \left[ \Theta_l(k) \Theta_{l'}(k') Y_{lm}^*(\hat{k}) Y_{l'm'}(\hat{k}') \right]. \quad (28)$$

This leads to,

$$\begin{aligned} A(l, l') = & -(4\pi T_0)^2 \int d^3k d^3k' (-i)^{l-l'+1} \delta^3(\vec{k}_-) g(k_+) \\ & \times \left\{ \Theta_l(k) \Theta_{l'}(k') \left[ \frac{-1}{k \sin \theta_k} Y_{l'm'}(\hat{k}') \frac{\partial}{\partial \theta_k} Y_{lm}^*(\hat{k}) + \frac{1}{k' \sin \theta_{k'}} Y_{lm}^*(\hat{k}) \frac{\partial}{\partial \theta_{k'}} Y_{l'm'}(\hat{k}') \right] \right. \\ & \left. + Y_{l'm'}(\hat{k}') Y_{lm}^*(\hat{k}) \left[ \frac{\partial \Theta_l(k)}{\partial k} \Theta_{l'}(k') \frac{k_z}{k} - \frac{\partial \Theta_{l'}(k')}{\partial k'} \Theta_l(k) \frac{k'_z}{k'} \right] \right\}, \end{aligned} \quad (29)$$

where  $\theta_k$  and  $\theta_{k'}$  are the polar angles of the vectors  $\vec{k}$  and  $\vec{k}'$  respectively. After integrating over  $k'$ , we can express this as,

$$A(l, l') = A_1(l, l') + A_2(l, l'), \quad (30)$$

where,

$$\begin{aligned} A_1(l, l') = & (-i)^{l-l'+1} (4\pi T_0)^2 \int d^3k g(k) \frac{\Theta_l(k) \Theta_{l'}(k)}{k \sin \theta_k} \\ & \times \left[ Y_{l'm'}(\hat{k}) \frac{\partial}{\partial \theta_k} Y_{lm}^*(\hat{k}) - Y_{lm}^*(\hat{k}) \frac{\partial}{\partial \theta_k} Y_{l'm'}(\hat{k}) \right], \end{aligned} \quad (31)$$

and

$$\begin{aligned} A_2(l, l') = & -(-i)^{l-l'+1} (4\pi T_0)^2 \int d^3k g(k) Y_{l'm'}(\hat{k}) Y_{lm}^*(\hat{k}) \frac{k_z}{k} \\ & \times \left[ \Theta_{l'}(k) \frac{\partial}{\partial k} \Theta_l(k) - \Theta_l(k) \frac{\partial}{\partial k} \Theta_{l'}(k) \right]. \end{aligned} \quad (32)$$

We compute  $A_1$  by directly using the formula for spherical harmonics,

$$Y_{lm}(\theta, \phi) = N_{lm} e^{im\phi} P_l^m(\cos \theta), \quad (33)$$

where,

$$N_{lm} = \sqrt{\frac{(2l+1)(l-m)!}{4\pi(l+m)!}}. \quad (34)$$

Integration over  $\phi$  in Eq. 31 leads to  $\delta_{mm'}$ . The conventions for the spherical harmonics, followed in HEALPIX [57], differ slightly from those used above. However this difference does not produce any change in our theoretical predictions. We, therefore, obtain,

$$A_1(l, l') = (-i)^{l-l'+1} 2\pi \delta_{mm'} (4\pi T_0)^2 N_{lm} N_{l'm} I_l \int dk k g(k) \Theta_l(k) \Theta_{l'}(k), \quad (35)$$

where,

$$I_l = \int_{-1}^1 dx \left[ P_l^m(x) \frac{d}{dx} P_{l'}^m - P_{l'}^m(x) \frac{d}{dx} P_l^m \right] = -2 \int_{-1}^1 dx P_{l'}^m(x) \frac{d}{dx} P_l^m. \quad (36)$$

This integral, for  $l' = l + 2n + 1$ ,  $n = 0, 1, 2, \dots$ , evaluates to [58],

$$I_l = -2 \left[ \delta_{0,m} - \frac{(l+m)!}{(l-m)!} \right]. \quad (37)$$

for  $m \geq 0$ . The corresponding result for  $m < 0$  can be easily determined by using this identity. The remaining  $k$  integral in  $A_1(l, l')$  has to be performed numerically. In the present paper we shall set,  $n = 0$ , and study only the correlations between  $l$  and  $l + 1$  multipoles. The model, however, also predicts higher order correlations, which require a more detailed study.

The integral  $A_2(l, l')$  can be expressed as,

$$\begin{aligned} A_2(l, l') &= -(-i)^{l-l'+1} (4\pi T_0)^2 \int dk k^2 d\Omega \cos \theta g(k) \\ &\times \left[ \Theta_{l'}(k) \frac{d}{dk} \Theta_l(k) - \Theta_l(k) \frac{d}{dk} \Theta_{l'}(k) \right] Y_{lm}^*(\hat{k}) Y_{l'm'}(\hat{k}). \end{aligned} \quad (38)$$

Using the identity,

$$\begin{aligned} \int d\Omega \cos \theta Y_{lm}^*(\hat{k}) Y_{l'm'}(\hat{k}) &= \delta_{mm'} \left[ \sqrt{\frac{(l-m+1)(l+m+1)}{(2l+1)(2l+3)}} \delta_{l',l+1} \right. \\ &\quad \left. + \sqrt{\frac{(l-m)(l+m)}{(2l+1)(2l-1)}} \delta_{l',l-1} \right], \end{aligned} \quad (39)$$

we obtain, for  $l' = l + 1$ ,

$$\begin{aligned} A_2(l, l') &= -\delta_{mm'} \sqrt{\frac{(l-m+1)(l+m+1)}{(2l+1)(2l+3)}} (4\pi T_0)^2 \\ &\times \int dk k^2 g(k) \left[ \Theta_{l'}(k) \frac{d}{dk} \Theta_l(k) - \Theta_l(k) \frac{d}{dk} \Theta_{l'}(k) \right]. \end{aligned} \quad (40)$$

Hence we find that the inhomogeneous power spectrum leads to a correlation between  $l$  and  $l \pm 1$ . This may be compared to the correlations, Eq. 5, we obtained from the dipole modulation model. The statistic  $S_H$  corresponding to the theoretical correlation, Eq. 25, is denoted as  $S_H^{theory}$ .

We set the homogeneous power,  $P(k) = k^{n-4} A_\phi / (4\pi)$ , where the parameters,  $n = 1$  and  $A_\phi = 1.16 \times 10^{-9}$  [55]. For the inhomogeneous term, we assume the form,

$$g(k) = g_0 P(k) \frac{(k\eta_0)^{-\alpha}}{\eta_0}. \quad (41)$$

Here  $g_0$  and  $\alpha$  are parameters. We have assumed that  $g(k)$  also has a power dependence on  $k$ , which is same as that of  $P(k)$  up to the extra term  $k^{-\alpha}$ . The precise combination  $(k\eta_0)$  is chosen since it is dimensionless. As explained above, the factor  $\eta_0$  is inserted in order make  $f_1(\Delta)$  and  $f_2(\Delta)$  have same dimensions. This implies that the constant  $g_0$  is dimensionless. This constant parameterizes the amplitude of inhomogeneity in the model. Using  $g(k)$ , we can compute  $A(l, l')$ . We obtain the theoretical prediction for correlations between multipoles  $l$  and  $l + 1$  by performing the integrals on the right hand sides of Eqs. 35 and 40 numerically. These can be used to obtain the theoretical estimate of the statistic for any value of the parameters,  $g_0$  and  $\alpha$ .

### III. DATA ANALYSIS

We use the cleaned CMB maps, WMAP's nine year ILC map (here after WILC9) [60] as well as the SMICA, provided by the PLANCK team [59]. For WILC9 map we use the  $KQ85$  mask and in the case of SMICA map, we use the CMB-union mask to eliminate the foreground contaminated regions. The masked portions are filled by simulated



random isotropic CMBR data. The cleaned SMICA map and the corresponding mask are provided at a high resolution with  $N_{side} = 2048$ . Hence in this case we generate a *foreground residual free* full sky CMB data map at this high resolution. Subsequently we downgrade this map to a lower resolution with  $N_{side} = 32$  after applying appropriate Gaussian beam to smooth the mask boundary [53]. This procedure eliminates any breaks that might be introduced at the boundary due to the random filling procedure. The WILC9 map is available only at lower resolution with  $N_{side} = 512$ . Hence the corresponding full sky map is generated only at this resolution and subsequently downgraded to a low resolution map with  $N_{side} = 32$ . In this case, the simulated map also includes the contribution due to detector noise. For PLANCK data, we do not include this contribution since the corresponding noise files are too bulky. As we shall see, for WMAP data, the detector noise gives very little contribution over the multipole range under consideration. This provides a good justification for neglecting the detector noise in our analysis. We also use the SMICA in-painted map, provided by the PLANCK team. This is a full sky map in which the masked regions have been reconstructed by the in-painting procedure [61, 62].

We use the three maps, described above, to determine the statistic,  $S_H(L)$ , over the multipole range  $2 \leq l \leq 64$ . This statistic is maximized by making a search over the preferred direction parameters, i.e. the choice of our z-axis. Due to the random filling of the masked regions, we obtain different results for different realizations for the full sky ‘data’ map. Hence the resulting quantities, i.e. maximum value of  $S_H(L)$  and the corresponding direction,  $(l, b)$ , are obtained by taking their average over 100 such filled data maps for the case of WILC9 and SMICA maps.

Our filling of masked regions with random isotropic data is likely to generate some bias in our results. We estimate this bias through simulations. The final results are obtained after making a correction for this bias. As we shall see this bias correction is relatively small. This procedure of bias correction through simulations is analogous to, for example, the procedure used in correcting for the residual foreground contamination in the ILC map by the WMAP science team [63]. We first simulate a full sky CMBR map which has same characteristics as the real data. This is obtained by the following steps:

1. We first generate a full sky random isotropic CMBR map.
2. The full sky map is multiplied by the dipole modulation term,  $(1 + A\hat{\lambda} \cdot \hat{n})$ , where the direction corresponds to that obtained by the WMAP five year analysis [5] and the amplitude is a free parameter. This creates a full sky realization of a simulated CMBR map which displays dipole modulation, as seen in the real data.
3. We next apply the same mask to this map as applied in the case of real data.
4. Finally the masked portions are filled with randomly generated isotropic CMBR data.

The above procedure generates a full sky realization of a map with same properties as the real map, including the dipole modulation. We now choose the amplitude  $A$  to be such that the final map leads to a statistic,  $S_H$ , same as that seen in real data,  $S_H^{data}$ . We perform this simulation by generating 1000 samples for a particular  $A$ . The output,  $S_H$ , is determined by taking the average over these samples. The error in  $S_H$  is given by the variance over these samples. This process is repeated over a large number of values of  $A$  in order to determine that value which leads to  $S_H$  closest to real data. The final  $A$ , determined by this procedure, gives us an estimate of the dipole modulation amplitude in real data, along with its error.

The final extracted value of  $A$  is used to determine the full sky estimate of the statistic. We use this value in order to generate 1000 full sky realizations of simulated CMBR maps, which have dipole modulation amplitude equal to the final extracted value of  $A$ . The statistic,  $S_H$ , computed by taking an average over these maps gives us an estimate of the full sky, bias corrected, statistic. As we shall see, the bias correction is relatively small.

The significance of anisotropy is determined by comparing the maximum value of bias corrected  $S_H(L)$  with that obtained from 4000 isotropic randomly generated full sky CMBR maps. The simulations used to estimate the significance from WILC9 map include detector noise, whereas those used for PLANCK data analysis ignore this contribution. The significance is quoted in terms of the P-value, which is defined as the probability that a random isotropic CMB map may yield a statistic larger than that seen in data. For each randomly generated map, we make a search over the direction parameters in order to maximize  $S_H(L)$ . The maximum values of 4000 random samples are compared with the data statistic. The P-value is estimated by counting the number of times the statistic of random data exceeds the observed data value. We point out that the significance is computed only as a consistency check. The main purpose of the present paper is to extract the dipole modulation amplitude and the parameters corresponding to the inhomogeneous power spectrum. In any case, as we shall see, our estimate of significance is in reasonable agreement with the significance obtained in literature [1, 2, 4] by hemispherical analysis.

The calculation is first performed over the entire range of multipoles,  $2 \leq l \leq 64$ , and then repeated over the three multipole bins,  $l = 2 - 22, 23 - 43, 44 - 64$ . Alternatively, we may determine  $A$  by using the formula, Eq. 5, for the correlation,  $\langle a_{lm} a_{l'm'}^* \rangle_{dm}$ , which is applicable for the dipole modulation model. We have verified that the value of  $A$  obtained by this formula agrees, within errors, with our direct simulations estimate.



We finally determine the inhomogeneous power spectrum i.e. the parameters,  $g_0$  and  $\alpha$ , defined in Eq. 41. We determine the theoretical prediction for the statistic,  $S_H(L)$ , using Eq. 25 for the correlation between different multipoles. We first extract the value of  $g_0$  for which the theoretical value of  $S_H$  matches the data value over the entire range of multipoles,  $2 - 64$ . In this case we set  $\alpha = 0$ . We next extract the values of  $g_0$  and  $\alpha$  by making a fit to the data statistic in the three multipole bins,  $l = 2 - 22, 23 - 43, 44 - 64$ , using the  $\chi^2$  minimization procedure. Here  $\chi^2$  is defined as,

$$\chi^2 = \sum_L \frac{[S_H^{theory}(L) - S_H^{data}(L)]^2}{[\delta S_H^{data}(L)]^2} \quad (42)$$

where the sum is over the three multipole bins. Here  $S_H^{theory}(L)$  is the theoretical estimate of the statistic in a particular multipole bin using the inhomogeneous model,  $S_H^{data}(L)$  the bias corrected estimate and  $\delta S_H^{data}(L)$  the corresponding error. In this case also we first set  $\alpha = 0$  and determine the best fit value of  $g_0$ . Next we determine both of these parameters.

#### IV. RESULTS

The extracted value of the data statistic,  $S_H^{data}$ , is given in Table I for the maps WILC9, SMICA and SMICA in-painted. This is obtained by searching over all possible directions in order to maximize  $S_H(L)$ . The corresponding direction parameters are found to be in good agreement with those found by using hemispherical anisotropy. For the case of WILC9 and SMICA we give both the raw and bias corrected values of  $S_H^{data}$ . The anisotropy is found to be significant roughly at  $3\sigma$  confidence level, which is in reasonable agreement with the estimate obtained by hemispherical analysis [1, 2, 5, 7]. In Table I, the significance is given in terms of the P-value, defined in section 3.

For the case of WILC9 the random realizations used to fill the masked regions as well as to generate simulated data include contribution due to the detector noise. If this contribution is not included, we find that the maximum value of  $S_H(L)$ , without applying bias correction, is also equal to  $0.023 \pm 0.007$ . It is same as the value given in Table I for WILC9. Hence the difference between the two cases is negligible. Furthermore the results of WMAP are in good agreement with those obtained by using PLANCK data. Hence we do not expect detector noise to be important in the multipole range of interest in this paper.

We next determine the value of the dipole modulation parameter,  $A$ , by comparing  $S_H^{data}$  with the statistic obtained by the simulated dipole modulated field over the range  $2 \leq l \leq 64$ . The best fit value of  $A$  for WILC9 is found to be  $0.090 \pm 0.029$ , and for SMICA,  $0.074 \pm 0.019$ . Hence the value matches well with that obtained by hemispherical analysis for the case of SMICA map [7]. For the case of WMAP [5], it is found to be a little larger. However the difference is not statistically significant.

As a consistency check we use Eq. 5 to determine the statistic, given our extracted value of  $A$ . Here we compute the right hand side of this equation by directly using the  $C_l$  values for different multipoles. This can be used to obtain an estimate of the statistic over the chosen multipole range, given a value of the dipole amplitude parameter,  $A$ . Using the value of  $A = 0.090 \pm 0.029$  for WMAP we obtain the value,  $S_H = 0.025 \pm 0.008$ , which is same as that given in Table I. For SMICA the corresponding value is  $S_H = 0.020 \pm 0.005$ , obtained by using  $A = 0.074 \pm 0.019$ , again in good agreement with the bias corrected value given in Table I.

Finally we extract the value of the amplitude,  $g_0$ , of the inhomogeneous term in the power spectrum which fits data over the entire multipole range,  $2 \leq l \leq 64$ . In this case we set the spectral index  $\alpha = 0$ . Comparison with data, leads to the value,  $g_0 = 0.087 \pm 0.028$  for WILC9 and  $g_0 = 0.077 \pm 0.020$  for SMICA. This corresponds to the value of  $g_0$  for which the theoretical value of the statistic matches the data value given in Table I.

	$S_H^{data}(L) (mK^2)$	$S_H^{data}(L) (mK^2)$ (bias corrected)	$(l, b)$	P-value
WILC9	$0.023 \pm 0.007$	$0.025 \pm 0.008$	$(227^\circ, -14^\circ)$	0.55%
SMICA	$0.021 \pm 0.005$	$0.023 \pm 0.006$	$(229^\circ, -16^\circ)$	2.6%
SMICA (in-painted)	$0.027 \pm 0.007$	—	$(232^\circ, -12^\circ)$	0.38%

TABLE I. The extracted value of  $S_H^{data}$  in the multipole range  $l = 2 - 64$ . This value is obtained from data after maximizing  $S_H(L)$  with a search over the direction parameters. The corresponding direction is given in galactic coordinates. The P-value represents the significance of the detected signal, as explained in text. For the case of SMICA (in-painted) no bias correction is required since here we directly use the full sky map.

We next study the variation of dipole modulation amplitude,  $A$ , with the multipole  $l$  using the map, WILC9. We divide data into 3 bins,  $l = 2 - 22, 23 - 43$  and  $l = 44 - 64$ , for this purpose. In each bin we determine the value of  $S_H^{data}$  and extract the best fit value of  $A(l)$ . For this analysis we found it convenient to fix the direction to be same as that obtained over the entire multipole range  $2 - 64$ . These direction parameters are also given in Table I. Alternatively, we may determine the best fit direction parameters, along with the amplitude, in each bin. We find that, in this case, the direction parameters show a mild dependence on the bin. The results for this case are shown in Table II and Table III for WILC9 and SMICA respectively. Since the dependence is relatively small, especially if we ignore the first bin, we fix the direction to be equal to the mean direction over the entire range. We next extract the values of  $S_H^{data}$  and  $A$  in the three multipole bins,  $l = 2 - 22, 23 - 43, 44 - 64$ , by repeating the entire procedure, including the bias analysis, described in section III. The resulting bias corrected values of  $S_H^{data}$  for WILC9 in the three bins,  $l = 2 - 22, 23 - 43$  and  $l = 44 - 64$ , are found to be  $0.0087 \pm 0.0057$ ,  $0.0082 \pm 0.0031$  and  $0.0061 \pm 0.0026$  respectively. The corresponding values for the SMICA map are found to be  $0.0084 \pm 0.0055$ ,  $0.0063 \pm 0.0033$  and  $0.0066 \pm 0.0032$  respectively. The extracted values of  $A$  are plotted in Fig. 1 for WILC9. We find that  $A$  shows a monotonic decrease with  $l$ . The results obtained with the SMICA and the SMICA in-painted map agree with those obtained with the WILC9 map within errors.

<i>multipole</i>	$A(l)$	$S_H^{data}(l)$	$(l, b)$
2 – 22	$0.134 \pm 0.068$	$0.011 \pm 0.006$	$(225^\circ, -65^\circ)$
23 – 43	$0.101 \pm 0.034$	$0.0092 \pm 0.0031$	$(229^\circ, 5^\circ)$
44 – 64	$0.076 \pm 0.028$	$0.0071 \pm 0.0026$	$(225^\circ, -25^\circ)$

TABLE II. The statistic  $S_H^{data}$  in the multipole range  $2 - 22, 23 - 43, 44 - 64$  and the corresponding direction parameters for WILC9. The extracted values of the effective dipole modulation parameter,  $A(l)$ , for these three bins are also shown.

<i>multipole</i>	$A(l)$	$S_H^{data}(l)$	$(l, b)$
2 – 22	$0.122 \pm 0.067$	$0.0101 \pm 0.0055$	$(228^\circ, -49^\circ)$
23 – 43	$0.074 \pm 0.034$	$0.0073 \pm 0.0034$	$(241^\circ, 3^\circ)$
44 – 64	$0.065 \pm 0.027$	$0.0074 \pm 0.0032$	$(221^\circ, -37^\circ)$

TABLE III. The extracted values of  $A(l)$ ,  $S_H^{data}$  and the direction parameters for SMICA.

We finally extract the function,  $g(k)$ , using data in the three multipole bins,  $l = 2 - 22, 23 - 43$  and  $l = 44 - 64$ . As explained above, the function,  $g(k)$ , is parametrized in terms of the overall constant,  $g_0$ , and the spectral index  $\alpha$ . We extract these two parameters by minimizing  $\chi^2$  in the three bins, as explained in section III. We first set  $\alpha = 0$  and determine  $g_0$  which best fits the data in the three bins. We obtain  $g = 0.075 \pm 0.020$  with  $\chi^2 = 0.50$  and  $g_0 = 0.070 \pm 0.023$  with  $\chi^2 = 0.22$  for WILC9 and SMICA respectively. Hence this provides a good fit to data. The data clearly favors a zero spectral index for the anisotropic part of the power spectrum. The resulting fit for WILC9 is shown in Fig. 2 as the dotted line. The value of  $\chi^2$  obtained by this fit is relatively small. However since we are fitting only three data points, such a low value is not unreasonable especially since the data in the first bin has a relatively large error. Allowing a non-zero value of  $\alpha$  we find that the  $1\sigma$  limit on this parameter is  $-0.34 < \alpha < 0.4$  for WILC9 and  $-0.24 < \alpha < 0.39$  for SMICA, that is consistent with zero. These limiting values are obtained by allowing  $g_0$  as a free parameter. The extracted values of  $g_0$  and  $\alpha$  with SMICA in-painted map are consistent with those quoted above.

## V. CONCLUSION

We have extended the results obtained in a recent paper [53], which showed that the dipole modulation model leads to correlations among spherical harmonic multipoles,  $a_{lm}$  and  $a_{l'm'}^*$  with  $m' = m$  and  $l' = l + 1$ . In that paper we defined a statistic,  $S_H$ , which provides a measure of this correlation in a chosen multipole range. By making a fit to this statistic in three multipole bins,  $l = 2 - 22, 23 - 43$  and  $l = 44 - 64$ , we find that the effective dipole modulation parameter  $A$  slowly decreases with the multipole,  $l$ .

We propose an inhomogeneous power spectrum model and show that it also leads to a correlation among different multipoles corresponding to  $m' = m$  and  $l' = l + 1$ , as in the case of the dipole modulation model. The inhomogeneous power spectrum is parameterized by the function,  $g(k)$ . We first fit the data by assuming that  $g(k)$  follows a purely scale invariant power spectrum, with  $\alpha = 0$  in Eq. 41. We determine the value of  $g_0$  by making a fit over the entire

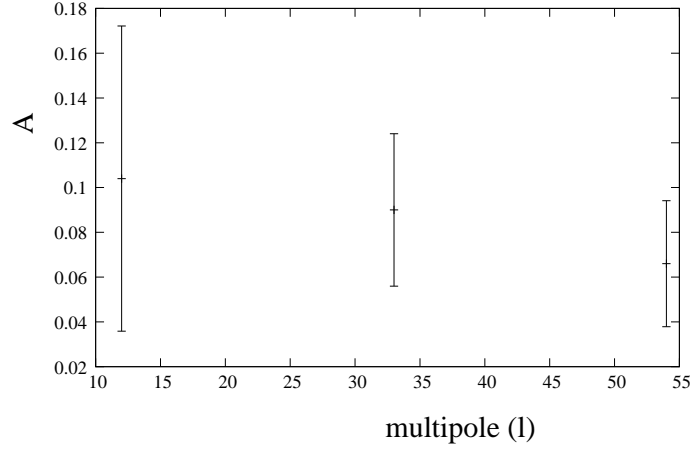


FIG. 1. The extracted value of the dipole modulation parameter,  $A$ , as a function of the multipole ( $l$ ), after fixing the direction parameters, for the three chosen multipole bins, 2 – 22, 23 – 43, 44 – 64.

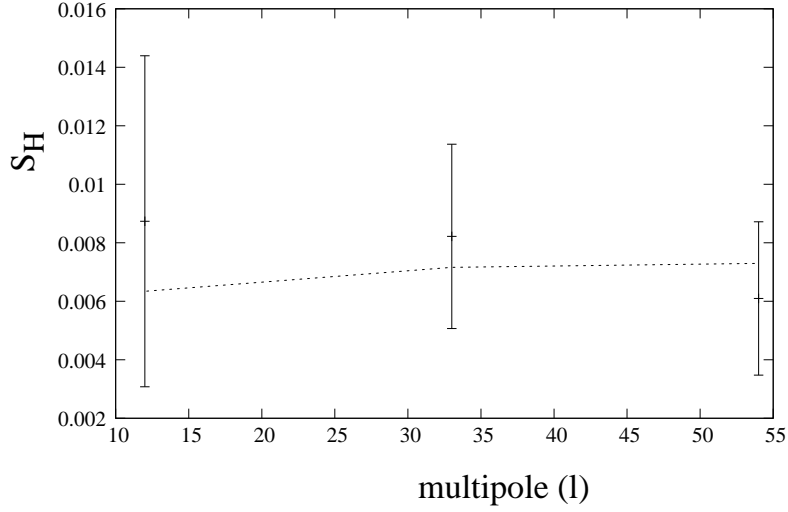


FIG. 2. The statistic,  $S_H^{data}$ , as a function of the multipole  $l$ . Here the statistic in the three bins is extracted by fixing the direction parameters to be equal to the mean direction over the entire multipole range. The dotted line represents the theoretical fit corresponding to  $\alpha = 0$ ,  $g_0 = 0.047 \pm 0.008$ .

multipole range, 2 – 64 for WILC9 and also SMICA . The best fit value for WILC9 is found to be  $g_0 = 0.087 \pm 0.028$  and in case of SMICA the value is  $g_0 = 0.077 \pm 0.020$ . We next make a fit over the three multipole bins, as in the case of the dipole modulation model. Again setting  $\alpha = 0$ , we obtain,  $g_0 = 0.075 \pm 0.020$ , with  $\chi^2 = 0.50$  and  $g_0 = 0.070 \pm 0.023$ , with  $\chi^2 = 0.22$  for WILC9 and SMICA respectively. Hence this provides a good fit to data and implies that the value of  $\alpha$  is consistent with zero. Allowing the parameter  $\alpha$  to vary, we find that the one sigma limit of  $\alpha$  for WILC9 and SMICA is  $-0.34 < \alpha < 0.40$  and  $-0.24 < \alpha < 0.39$  respectively.

## VI. APPENDIX A

In this appendix we derive Eq. 28. We first change the integration variables from  $\vec{k}, \vec{k}'$  to  $\vec{k}_-, \vec{k}_+$  in Eq. 27. The Jacobian of this transformation is unity. We next integrate Eq. 27 by parts over the variable  $k_{-z}$ . We obtain,

$$A(l, l') = -(4\pi T_0)^2 \int d^3 k_- d^3 k_+ (-i)^{l-l'+1} \delta^3(\vec{k}_-) g(k_+) \frac{\partial}{\partial k_{-z}} \left[ \Theta_l(k) \Theta_{l'}(k') Y_{lm}^*(\hat{k}) Y_{l'm'}(\hat{k}') \right] + \bar{A}(l, l') \quad (43)$$

where  $\bar{A}(l, l')$  is the surface term,

$$\bar{A}(l, l') = (-i)^{l-l'+1} (4\pi T_0)^2 \int d^3 k_+ dk_{-x} dk_{-y} B(l, l') \quad (44)$$

and

$$B(l, l') = \int_{-\infty}^{\infty} dk_{-z} \frac{\partial}{\partial k_{-z}} \left[ \delta^3(\vec{k}_{-}) g(k_+) \Theta_l(k) \Theta_{l'}(k') Y_{lm}^*(\hat{k}) Y_{l'm'}(\hat{k}') \right] \quad (45)$$

In order to evaluate this we use a standard representation of the delta function, given by,

$$\delta(x) = \lim_{\epsilon \rightarrow 0^+} \frac{1}{2\sqrt{\pi\epsilon}} e^{-x^2/(4\epsilon)} \quad (46)$$

We may now express  $B(l, l')$  as,

$$B(l, l') = \lim_{\epsilon \rightarrow 0^+} \frac{1}{2\sqrt{\pi\epsilon}} \lim_{K \rightarrow \infty} \int_{-K}^K dk_{-z} \frac{\partial}{\partial k_{-z}} \left[ \delta(k_{-x}) \delta(k_{-y}) e^{-k_{-z}^2/(4\epsilon)} g(k_+) \Theta_l(k) \Theta_{l'}(k') Y_{lm}^*(\hat{k}) Y_{l'm'}(\hat{k}') \right] \quad (47)$$

As we perform the integral over  $k_{-z}$  the term in bracket gets evaluated at  $k_{-z}^2 = K^2 \rightarrow \infty$  at both the upper and lower limit of the integral. Hence this term is proportional to  $\exp(-\infty)$  which is equal to zero. For the remaining term in Eq. 43, we change the integration variables back to  $\vec{k}, \vec{k}'$ . This gives us Eq. 28.

**Acknowledgments:** Some of the results in this paper have been derived using the Healpix package [57]. We are grateful to James Zibin for a very useful communication and thank Shamik Ghosh for useful comments. Finally we acknowledge the use of Planck data available from NASA LAMBDA site (<http://lambda.gsfc.nasa.gov>).

- 
- [1] H. K. Eriksen et al., ApJ **605**, 14 (2004).
  - [2] H. K. Eriksen et al., 2007, ApJL **660**, L81 (2007).
  - [3] A. L. Erickcek, M. Kamionkowski, and S. M. Carroll, Phys. Rev. D **78**, 123520 (2008).
  - [4] F. K. Hansen et al., ApJ **704**, 1448 (2009).
  - [5] J. Hoftuft et al., ApJ, **699**, 985 (2009).
  - [6] F. Paci et al., MNRAS **434**, 3071 (2013).
  - [7] P. Ade, et al., Planck 2013 results - XXIII [arXiv:1303.5083]
  - [8] F. Schmidt and L. Hui, Phys. Rev. Lett. **110**, 011301 (2013).
  - [9] Y. Akrami et al., ApJL **784**, L42 (2014).
  - [10] C. Gordon et al., Phys. Rev. D **72**, 103002, (2005).
  - [11] C. Gordon, ApJ **656**, 636 (2007).
  - [12] S. Prunet et al., Phys. Rev. D **71**, 083508 (2005).
  - [13] C. Bennett et al., ApJS **192**, 17 (2011).
  - [14] E. P. Donoghue and J. F. Donoghue, Phys. Rev. D **71**, 043002 (2005).
  - [15] D. Hanson and A. Lewis, Phys. Rev. D **80**, 063004 (2009).
  - [16] C. M. Hirata, JCAP **09**, 011 (2009).
  - [17] R. Fernandez-Cobos et al., 2013 [arXiv:1312.0275]
  - [18] A. L. Erickcek, C. M. Hirata and M. Kamionkowski, Phys. Rev. D **80**, 083507 (2009).
  - [19] D. Hutsemekers, A & A **332**, 410 (1998).
  - [20] P. Jain and J. P. Ralston, Mod. Phys. Lett. A **14**, 417 (1999).
  - [21] A. de Oliveira-Costa et al., Phys. Rev. D **69**, 063516 (2004).
  - [22] J. P. Ralston and P. Jain, Int. Jou. Mod. Phys. D **13**, 1857 (2004).
  - [23] D. J. Schwarz et al, Phys. Rev. Lett. **93**, 221301 (2004).
  - [24] A. K. Singal, ApJL, **42**, L23 (2011).
  - [25] P. Tiwari and P. Jain, 2013 [arXiv:1308.3970]
  - [26] A. Berera, R. V. Buniy and T. W. Kephart, JCAP **10**, 016 (2004).
  - [27] L. Ackerman, S. M. Carroll and M. B. Wise, Phys. Rev. D **75**, 083502 (2007).
  - [28] C. G. Boehmer and D. F. Mota, Phys. Lett. B **663**, 168 (2008).
  - [29] T. R. Jaffe et al., ApJ **644**, 701 (2006).
  - [30] T. Koivisto and D. F. Mota, Phys. Rev. D **73**, 083502 (2006).
  - [31] K. Land and J. Magueijo, MNRAS **367**, 1714 (2006).
  - [32] M. Bridges et al., MNRAS **377**, 1473 (2007).

- [33] L. Campanelli, P. Cea and L. Tedesco, Phys. Rev. D **76**, 063007 (2007).
- [34] T. Ghosh, A. Hajian and T. Souradeep, Phys. Rev. D **75**, 083007 (2007).
- [35] A. Pontzen and A. Challinor, MNRAS **380**, 1387 (2007).
- [36] T. Koivisto and D. F. Mota, JCAP **08**, 021 (2008).
- [37] T. Kahniashvili, G. Lavrelashvili and B. Ratra, Phys. Rev. D **78**, 063012 (2008).
- [38] S. M. Carroll, C.-Y. Tseng and M. B. Wise, Phys. Rev. D **81**, 083501 (2010).
- [39] M. Watanabe, S. Kanno and J. Soda, Prog. Theo. Phys. **123**, 1041 (2010).
- [40] Z. Chang and S. Wang, Eur. Phys. Jour. C **73**, 2516 (2013).
- [41] L. Wang and A. Mazumdar, Phys. Rev. D **88**, 023512 (2013).
- [42] A. Mazumdar and L. Wang, JCAP **10**, 049 (2013).
- [43] Y.-F. Cai, W. Zhao and Y. Zhang, Phys. Rev. D **89**, 023005 (2014).
- [44] Z.-G. Liu, Z.-K. Guo and Y.-S. Piao, Phys. Rev. D **88**, 063539 (2013).
- [45] Z. Chang, X. Li and S. Wang, 2013 [arXiv:1307.4542]
- [46] Z. Chang and S. Wang, 2013 [arXiv:1312.6575]
- [47] P. Aluri, S. Panda, M. Sharma and S. Thakur, JCAP **1312**, 003 (2013).
- [48] J. McDonald, 2014 [arXiv:1403.2076]
- [49] S. Ghosh S., Phys. Rev. D **89**, 063518 (2014).
- [50] S. Panda, M. Sharma, arXiv:1406.3992.
- [51] P. K. Aluri and P. Jain, Mod. Phys. Lett. A **27**, 1250014 (2012).
- [52] P. K. Rath et al., JCAP **04**, 007 (2013).
- [53] P. K. Rath and P. Jain, JCAP **12**, 014 (2013).
- [54] X. Gao, Phys. Lett. B **702**, 12 (2011).
- [55] D. S. Gorbunov and V. A. Rubakov, *Introduction to the Theory of the Early Universe : Cosmological Perturbations and Inflationary Theory*, World Scientific (2011)
- [56] L. R. Abramo and T. S. Pereira, Advances in Astronomy, 378203 (2010).
- [57] K. Gorski et al., ApJ **622**, 759 (2005).
- [58] S. N. Samaddar, Mathematics of Computation, **28**, No. 125, p257 (1974).
- [59] P. Ade et al., Planck 2013 results - I [arXiv:1303.5062]
- [60] C. L. Bennett et al., APJS **208**, 20 (2013).
- [61] P. Abrial et al., Statistical Methodology **5**, 289 (2008).
- [62] K. T. Inoue, P. Cabella and E. Komatsu, Phys. Rev. D **77**, 123539 (2008).
- [63] G. Hinshaw et al., ApJS **170**, 288 (2007).